RESEARCH ARTICLE OPEN ACCESS

BTISS-WNET: Deep Learning-based Brain Tissue Segmentation using Spatio-Temporal WNET

Athur Shaik Ali Gousia Banu®, and Sumit Hazra®

Department of Computer Science and Engineering, Koneru Lakshmiah Education Foundation, Hyderabad, Telangana, India.

Corresponding author: Athur Shaik Ali Gousia Banu. (e-mail: gbanuzia@gmail.com), **Author(s) Email**: Sumit Hazra (sumit.hazra@klh.edu.in)

Abstract Brain tissue segmentation (BTISS) from magnetic resonance imaging (MRI) is a critical process in neuroimaging, aiding in the analysis of brain morphology and facilitating accurate diagnosis and treatment of neurological disorders. A major challenge in BTISS is intensity inhomogeneity, which arises from variations in the magnetic field during image acquisition. This results in non-uniform intensities within the same tissue class, particularly affecting white matter (WM) segmentation. To address this problem, we propose an efficient deep learning-based framework, BTISS-WNET, for accurate segmentation of brain tissues. The main contribution of this work is the integration of a spatio-temporal segmentation strategy with advanced pre-processing and feature extraction to overcome intensity inconsistency and improve tissue differentiation. The process begins with skull stripping to eliminate non-brain tissues, followed by Empirical Wavelet Transform (EWT) for noise reduction and edge enhancement. Data augmentation techniques, including random rotation and flipping, are applied to improve model generalization. The preprocessed images are fed into Res-GoogleNet (RGNet) to extract deep semantic features. Finally, a Spatio-Temporal WNet is used for precise WM segmentation, leveraging spatial and temporal dependencies for improved boundary delineation. The proposed BTISS-WNET model achieves a segmentation accuracy of 99.32% for white matter. It also demonstrates improved accuracy of 1.76%, 18.23%, and 16.02% over DDSeg, BISON, and HMRF-WOA, respectively. In conclusion, BTISS-WNET provides a robust and high-accuracy framework for WM segmentation in MRI images, with promising applications in clinical neuroimaging. Future work will focus on validating the model using real clinical datasets and extending it to multi-tissue and multi-modal MRI segmentation.

Keywords MRI Images; Brain Tissue Segmentation; Empirical wavelet transformer; Res-GoogleNet; Deep learning.

I. Introduction

Brain Tissue Segmentation (BTISS) is a prominent research area in medical image processing, focused on accurately categorizing and defining tumor regions in brain MRI. [1]. Tissue is extracted from a brain image by separating it into disjoint regions that share common characteristics, such as homogeneity in intensity and texture [2]. There are five general categories of brain BTISS methods: manual, region-based, clusteringbased, thresholding-based, and feature extraction and classification-based [3]. BTISS methods are also affected by several factors, like location, size, texture, shape, and unclear tissue boundary, which are inherent to the modalities used to acquire images [4]. WM lesion quantification is required for medication therapy evaluation in multiple sclerosis. Α qualified multidisciplinary medical board is involved in the decision-making process [5]. Deep learning (DL)-based automatic segmentation techniques offer notable benefits over conventional techniques in terms of processing efficiency and accuracy [6]. By precisely identifying brain regions of interest and distinguishing them from healthy brain tissue, the DL techniques enable more precise quantitative analysis [7], [8].

Additionally, DL-based techniques have made significant progress in segmenting brain tissue, including that of fetuses, newborns, and adults [9]. Despite brain MRI's intricacy and intensity fluctuations, BTISS still faces numerous difficulties [10], [11]. However, because of the intricate architecture and intensity fluctuations in brain MRI, tissue segmentation is difficult to achieve. Accurate segmentation using MRI is still a difficult undertaking to diagnose and treat patients more successfully [12]. At the moment, there

1

Manuscript received Marc 8, 2025; Revised August 20, 2025; Accepted September 1, 2025; date of publication December 4, 2025 Digital Object Identifier (**DOI**): https://doi.org/10.35882/jeeemi.v8i1.808

Copyright © 2025 by the authors. This work is an open-access article and licensed under a Creative Commons Attribution-ShareAlike 4.0 International License (CC BY-SA 4.0).

Journal of Electronics, Electromedical Engineering, and Medical Informatics

Homepage: jeeemi.org; Vol. 8, No. 1, January 2026, pp: 1-15 e-ISSN: 2656-8632

is insufficient training data required for precise segmentation, which could result in the segmentation model's poor generalizability [13], [14]. Furthermore, the intricacy and variety of brain tissue structures numerous challenges for segmentation [15]. To overcome this, a novel BTISS-WNET is proposed for BTISS using MRI images. The proposed BTISS-WNET introduces a novel hybrid segmentation framework that integrates three core components: EWT for pre-processing, RGNet for feature extraction, and Spatio-temporal WNet for segmentation. The integration of EWT, RGNet, and Spatio-temporal WNet establishes a new standard in MRI BTISS by addressing key limitations in noise suppression, multi-scale feature extraction, and spatiotemporal continuity. This hybrid architecture not only surpasses traditional segmentation methods in terms of accuracy but also enhances structural preservation, especially in challenging WM regions. The key contributions of this work are summarized as,

- 1. Initially, the skull is removed from the brain MRI images by skull stripping, and EWT pre-processes the images to enhance the image and reduce noise.
- The augmented MRI images are input to the RGNet, a hybrid network that combines ResNet and GoogleNet architectures for efficient feature extraction.
- These features are fed into the Spatio-temporal WNet model to segment the WM in the brain MRI, leveraging temporal data and spatial attention mechanisms for enhanced accuracy and precision in segmentation.
- The performance of the proposed model was measured by some specific metrics like specificity (SP), F1 score (F1), precision (PR), recall (RE), accuracy (AC), Jaccard index (JI), and dice score (DI).

The structure of the paper is planned as follows: section 2 defines the literature survey, section 3 explains the proposed BTISS-WNET, section 4 includes the final results, and section 5 defines the ablation study. Section 6 shows the discussion part. Lastly, the conclusion enfolds in section 7.

II. Literature Review

Recently, a number of DL-based techniques for BTISS have been made available to help radiologists do more precise diagnostic evaluations. Some of the most current studies are compiled in this area.

In 2020, Yamanakkanavar, N. et al. [16] suggested a M-net architecture for BTISS automatically. The encoder and decoder modules employ dilated convolutional kernels of varying sizes to capture semantic information from the MRI. The suggested M-net offers improved fine detail retention while overcoming the shortcomings of traditional techniques.

The suggested M-net has a high computational complexity due to the use of multiple dilated convolutional kernels. The BTISS-based medical decision support approach was proposed by Veluchamy, M. et al. in 2021 [17]. The modified brain MRI was then segmented using a personalized fuzzy c-means clustering technique. The results of the experiments show that this suggested model handles the inhomogeneity of intensity and noise well. The BTISS-based approach relies on manual parameter tuning, which may affect segmentation consistency across diverse datasets. Cleriques, A., et al. [18] proposed a 3D patch-based DL architecture for BTISS in 2023. The multi-task U-Net design, end-to-end inpainting, and system segmentation reduce WM lesions. Effective WM lesion reduction is achieved by the multi-task U-Net with the end-to-end inpainting and segmentation procedure. The model performance may degrade when applied to datasets with low contrast between lesions and surrounding tissue. A multi-scale Highlighting Foregrounds U-Net was proposed in 2021 for the BTISS by Park, G., et al. [19], U-Net aims to expand the identification of WMH pixels with partial volume effects. Among the 39 techniques presented in the WMH Segmentation, the suggested approach has the dice similarity index (DI) and F1-score. The proposed multi-scale Highlighting Foregrounds U-Net reduced accuracy in segmenting small or low-contrast WMH regions due to reliance on intensity variations.

M-SeaNet architecture presented Yamanakkanavar, N et al. [20] for BTISS received worldwide attention in 2021. During decoding, global attention integrates local features with their global dependencies to collect rich contextual information. proposed model outperforms traditional techniques in experimental data, with an average DI of 0.96. The M-SegNet model is the integration of global which increase attention, may computational complexity, making real-time processing challenging. Rieu et al. (2021) suggested a semi-supervised method for BTISS [21]. The reference labels acquired using FreeSurfer segmentation on T1w MRI were compared with the outcomes of the proposed technique. The proposed BTISS can be evaluated by comparing the outcomes of the suggested method with the DI. The proposed reliance on FreeSurfer-generated labels introduces bias due to potential inaccuracies in its automated segmentation. An optimum support vector machine for classifying and segmenting MRI brain tumors was proposed by Kollem, S., et al. in 2024 [22]. The contourlet transform utilizes a dual filter consisting of a Laplacian pyramid and a directional filter bank to generate a sparse representation of smooth contours. The extracted bands are segmented utilizing Possibility Fuzzy C-Means and clustering method. The method struggles with accurately segmenting tumors in images with low contrast levels.

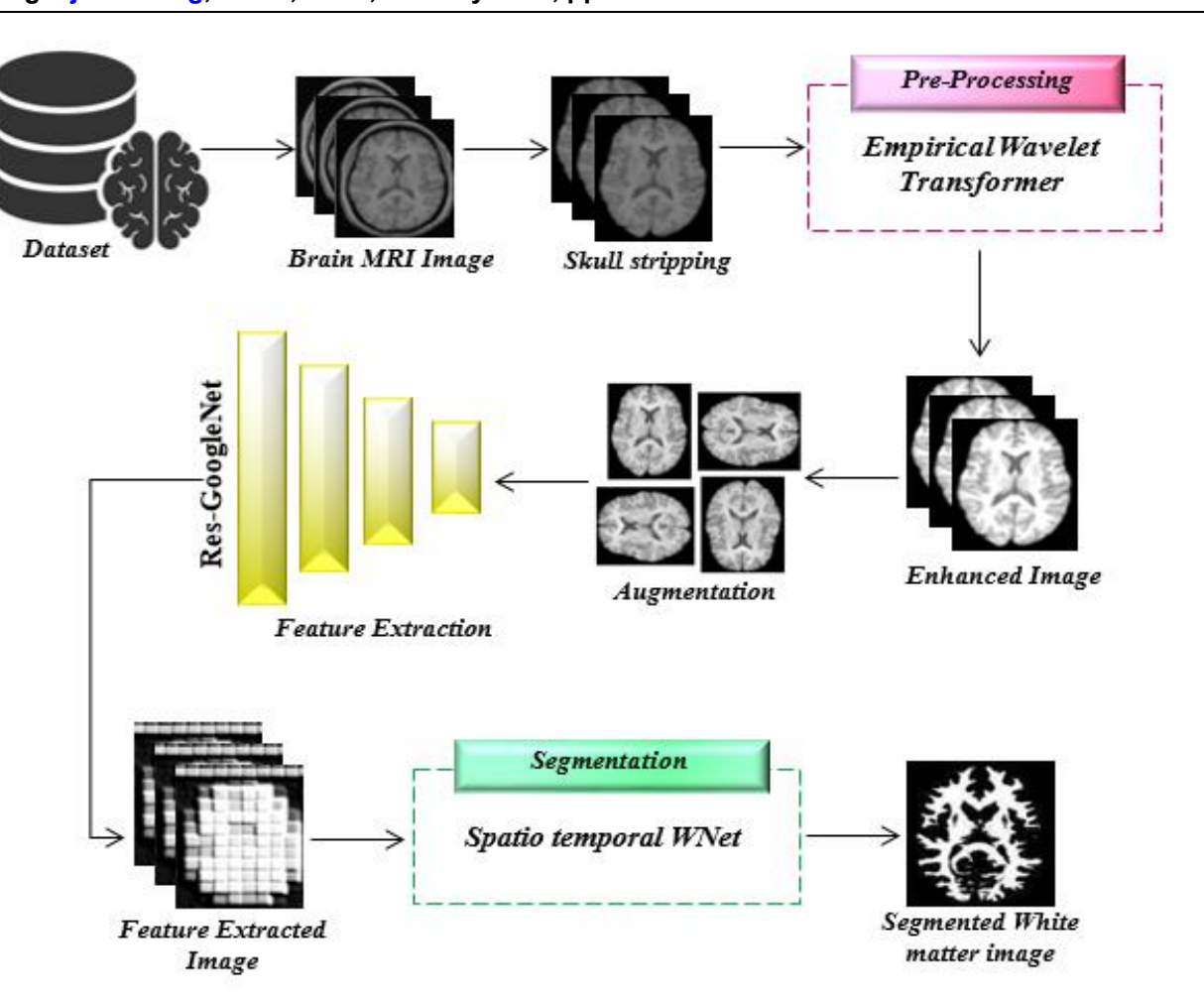


Fig. 1. Proposed BTISS-WNET methodology

In 2024, Kollem, S., et al. introduced an optimal support vector machine designed to classify and segment MRI brain tumors [23]. The suggested approach is capable of managing noise, PVE, and IIH. The Firefly method (FA) and a chaotic map are used in conjunction with a spatially modified FCM method called CEFAFCM to initialize the firefly population. Brain MRIs obtained from the BrainWeb database are used to test the algorithm. The method relies heavily on the quality of initialization, which may impact performance in complex tumor regions.

From this literature, the existing techniques exhibit several limitations on BTISS using different ML and DL models. A major challenge in BTS is intensity inhomogeneity in MRI images. This occurs due to variations in the magnetic field during image acquisition, leading to non-uniform intensity across the same tissue type. To overcome these problems, a novel BTISS-WNET is proposed for WM segmentation.

III. Proposed BTISS-WNET

In this paper, a novel BTISS-WNET is suggested for BTISS. The MRI is fed into skull stripping to remove

skull regions, and EWT is used for pre-processing to expand image quality and noise reduction. The augmented MRI images of the brain are fed into RGNet for extracting the fine features. The proposed method uses Spatio-temporal WNet for segmenting the WM in brain MRI images. The proposed methodology is displayed in Fig. 1.

A. Dataset Description

Brain MRI scans are sourced from the BrainWeb dataset. The popular synthetic MRI dataset BrainWeb provides controlled situations with different intensity non-uniformities and noise levels. Important features are RF inhomogeneity levels of 0%, 20%, and 40%, which simulate intensity non-uniformities, and noise levels of 0%, 1%, 3%, and 5%. A training set contains 36 images from all noise levels and RF levels, a validation set encompasses 12 images, and a test set comprises 57 images.

B. Empirical Wavelet Transformer

An empirical wavelet transform [24] enables a signal to be adaptively extracted into different modes.

This method uses a succession of wavelet filters to extract all modes, assuming that each mode's Fourier spectrum has compact support. Based on Meyer's

wavelets and Littlewood-Paley Eq. (1), Eq. (2) [24] defines the Fourier spectra of a scaling function.

$$\varphi_{n}(\omega) = \begin{cases} 1 & |\omega| \leq (1 - \gamma)\omega_{n} \\ \cos\left[\frac{\pi}{2}\beta\left(\frac{1}{2\gamma\omega_{n}}(|\omega| - (1 - \gamma)\omega_{n})\right)\right] & (1 - \gamma)\omega_{n} \leq |\omega| \leq (1 + \gamma)\omega_{n} \\ 0 & others \end{cases}$$
(1)

$$\psi_{n}(\omega) = \begin{cases}
1 & (1+\gamma)\omega_{n} \leq |\omega| \leq (1-\gamma)\omega_{n+1} \\
\cos\left[\frac{\pi}{2}\beta\left(\frac{1}{2\gamma\omega_{n+1}}(|\omega| - (1-\gamma)\omega_{n+1})\right)\right] & (1-\gamma)\omega_{n+1} \leq |\omega| \leq (1+\gamma)\omega_{n+1} \\
\sin\left[\frac{\pi}{2}\beta\left(\frac{1}{2\gamma\omega_{n}}(|\omega| - (1-\gamma)\omega_{n+1})\right)\right] & (1+\gamma)\omega_{n} \leq |\omega| \leq (1+\gamma)\omega_{n+1} \\
0 & others
\end{cases} \tag{2}$$

In Eq. (1), ω denotes omega, β represents the beta, γ defines the gamma, $\varphi_n(\omega)$ is the frequency response of the filter function for band index n at angular frequency ω , ω is the Angular frequency variable, ω_n is

$$W_f(0,t) = [f(t), \overline{\varphi_1(\tau - t)}d\tau = IFT(FT(f(\tau)) \times \overline{\varphi_1(\omega)})$$
(3)

defined as the center frequency of the n^{th} filter, γ is the bandwidth parameter, $\beta(.)$ is a smooth transition function. In Eq. (2), $\psi_n(\omega)$ denotes the Frequency response of the n^{th} band-pass filter, ω_n, ω_{n+1} defines the Center frequencies of the n^{th} and $n+1^{th}$ filters, γ represents the Bandwidth smoothing parameter controlling the width of the transition band.

In Eq. (3) [24], f(t) represents the original signal, $\varphi_1(\tau-t)$ denotes the kernel function centered at time t, and the $\overline{(.)}$ denotes complex conjugation. $FT(f(\tau))$

$$W_f(n,t) = [f(t), \overline{\psi_n(\tau - t)}d\tau = IFT\left(FT\left(f(\tau)\right) \times \overline{\varphi_n(\omega)}\right)$$

denotes the Fourier Transform of the signal f. $\overline{\varphi_1(\omega)}$ represents the complex conjugate of the Fourier Transform of the window φ_1 and IFT denotes the Inverse Fourier Transform. In Eq. (4) [24] $W_f(n,t)$ represents the wavelet coefficient at scale n and time shift t, $\psi_n(\tau - t)$ represents the wavelet function at scale n shifted to be centered at time t. FT stands for the Fourier transform, and IFT for the inverse Fourier transform, \times is the convolution operator and $\overline{(.)}$ for the complex conjugate operator.

C. Augmentation

This study uses various augmentation methods to supplement the improved data. Enhancing the diversity of training dataset samples over data augmentation can improve the performance and output of DL methods. Affine image processing and image augmentation approaches are active to increase the size of the training database. The pre-processed

(3) adaptively decompose a signal f(t) for analysis using the previously given equations. where the scale function inner product determines the approximation

coefficients, W_f (0, t), and the wavelet inner product

determines the detail coefficients, Wf (n, t):

 $\beta(\omega)$ is defined as follows: $\beta(\omega) = \omega^4(35 - 84\omega +$

scaling function's frequency support and wavelets'

frequency support should be tight. It is possible to

images were exposed to various augmentation methods to increase generalization and avoid overfitting of the object detection model. Several image

augmentation methods, such as multi-angle rotation, adding Gaussian noise, improving and reducing brightness, and horizontal and vertical mirroring, were used to increase the categorization AC. The 1200 images that each class submitted are divided into 400 testing images and 800 training each class images. to create a diversity of images for testing and training, an image augmentation technique called a factor of 10 was utilized.

D. Res-Googlenet

The augmented MRI images of the brain are fed into RGNet for extracting the features from the images. Fig. 2 displays the architecture of Res-GoogleNet. Res-Googlenet is a hybrid model combining GoogleNet (Inception Modules) and ResNet (Residual Learning) [26] for enhanced feature extraction. In the hybrid model, the 177 levels were eliminated, and ten additional layers were created to take their place,

(4)

bringing the total number of layers to 182. The idea of conception modules was first presented by the CNN architecture. 1x1, 3x3, 5x5 convolutions, and 3x3 max pooling are among the processes included in the Inception modules. Reducing the data input size for the next laver is the primary goal of pooling. Two popular techniques are Maximum Pooling and Average Pooling. The filters in the pooling layer are selected using NxN dimensions. A 1x1 convolution reduces the number of output volume channels. Consequently, the architecture was able to outperform other deep CNN with fewer parameters in terms of computational efficiency. An entirely densely linked layer sits parallel to two conv layers in the Dense-Inception [25] structure, an adaptation of the Inception architecture. While the fully dense connection guarantees the completeness of the information, we decrease its depth to decrease the number of parameters. The Inception concatenates the results of several convolutions (1x1,

[27] introduces skip connections, allowing gradients to flow through the network more effectively. For a given input x, the residual block is defined as Eq. (6) [27]:

$$\mathcal{F}_{residual}(x) = x + \mathcal{F}(x, W_i)$$
 (6)

Here, x is the feature map, $\mathcal{F}(x,W_i)$ is the residual mapping, which is the output of the conv layers and W_i is the weights of the conv filters. The residual connection bypasses the conv path, ensuring stable gradient propagation during backpropagation. In ResGoogleNet, the inception is embedded within a residual block [28], so the overall mapping is,

$$y = x + \mathcal{F}_{inception}(x) \tag{7}$$

In Eq. (7) [28], y is the output of the ResGoogleNet block and $\mathcal{F}_{inception}(x)$ is the output from the inception module. When stacking multiple layers, the final output after n layers of ResGoogleNet becomes:

$$y^{[n]} = x + \sum_{i=1}^{n} \mathcal{F}_{inception}^{[i]}(x)$$
 (8)

In Eq. (8) [28], cumulative representation captures

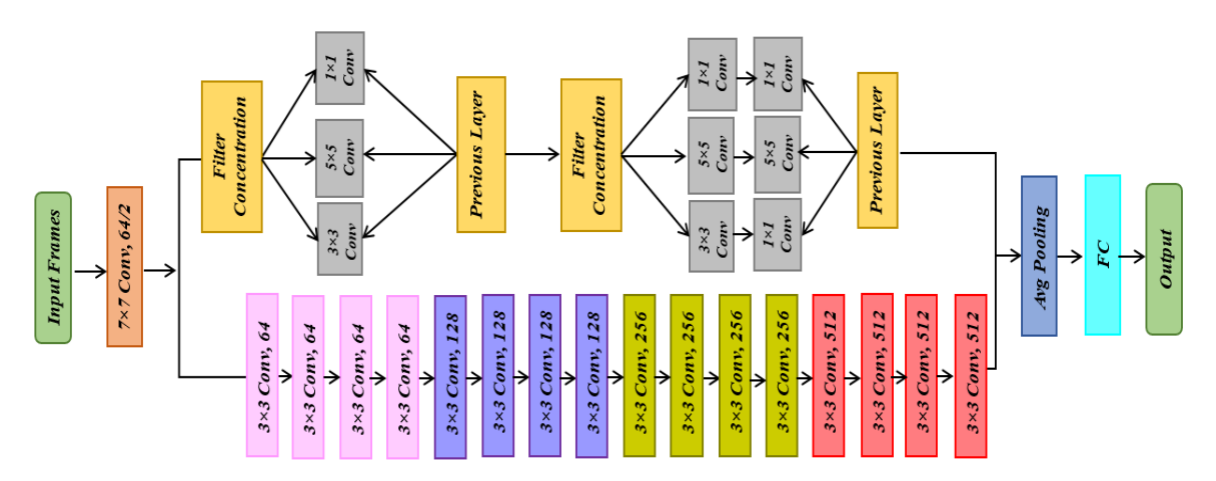


Fig. 2. Architecture diagram of Res-GoogleNet

3x3, 5x5) and pooling operations that are carried out concurrently in Eq. (5) [26]:

This notation indicates that a pooling layer and several conv layers are applied to the input x at the

hierarchical features, enhancing boundary detection and tissue differentiation in MRI segmentation. where, $y^{[n]}$ denotes the final cumulative output, x represents

$$\mathcal{F}_{Incention}(x) = [Conv_{1\times 1}(x) \oplus Conv_{3\times 3}(x) \oplus Conv_{5\times 5}(x) \oplus Maxpooling(x)] \tag{5}$$

same time. Then, along the channel dimension, the outputs are concatenated. Maxpooling(x) defines the max pooling operation that reduces the spatial dimensions while keeping dominant features. \bigoplus Denotes channel-wise concatenation of the parallel outputs, combining multi-scale information into a unified feature representation. This multi-branch structure enables ResGoogleNet to capture features of varying spatial resolutions. Utilizing the Inception module as the residual function $\mathcal F$ in a residual block is the fundamental principle of ResGoogleNet. ResNet

the original input feature map, $\sum_{i=1}^{n} \mathcal{F}_{inception}^{\lfloor i \rfloor}(x)$ defines the summation of outputs from multiple Inception modules, each applied to the same input x, $\mathcal{F}_{inception}^{\lfloor i \rfloor}$ denotes output of the i^{th} Inception block. Res-Googlenet serves as the feature extraction backbone, generating detailed spatial features before segmentation by the Spatio-temporal WNet.

E. Spatio Temporal WNet

In this section, the Spatio-Temporal WNet is used to segment the WM from the extracted MRI images.

A spatiotemporal [29] model includes spatial and temporal properties as well as data collected across space and time. In the W-Net architecture, a CNN and

transformer-based backbone network is used, similar to the U-Net architecture for segmenting WM. Fig. 3 shows the Spatio-Temporal WNet architecture.

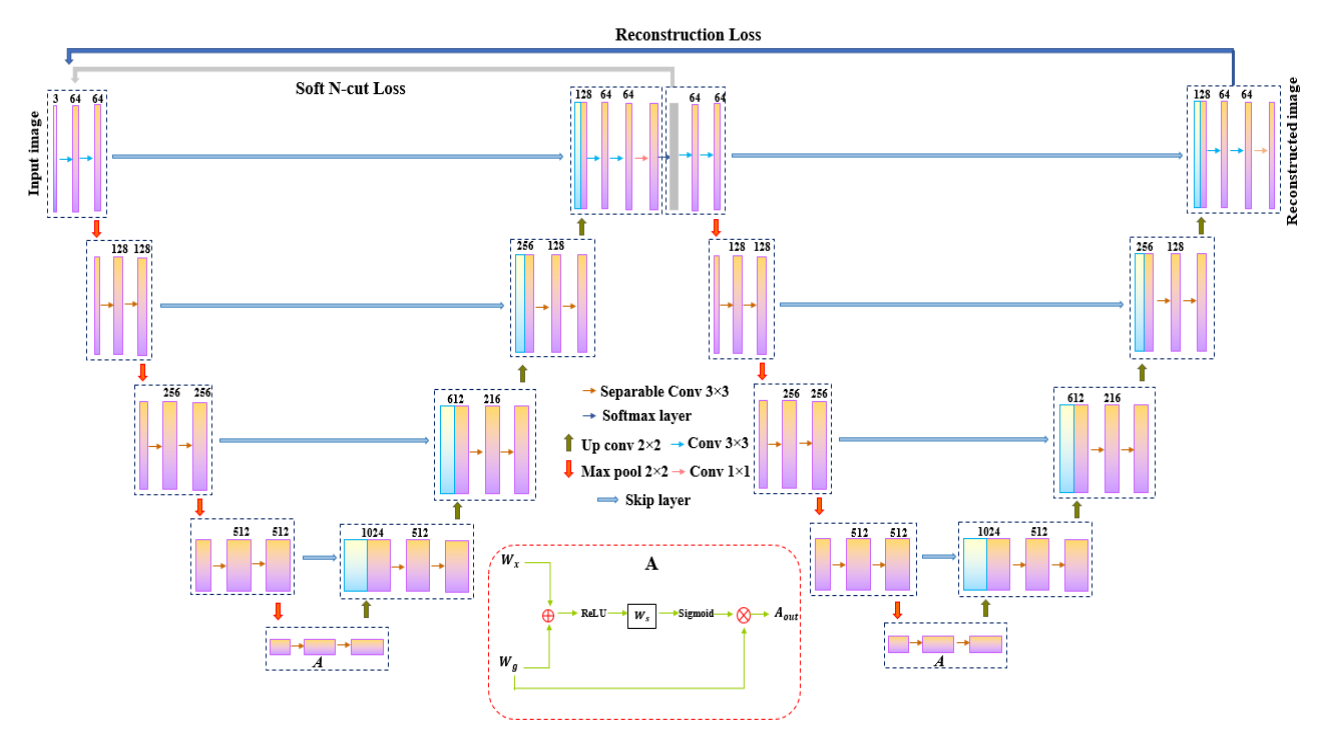


Fig. 3. Architecture diagram of Spatio temporal WNet

A W-Net consists of 18 modules with two 3x3 conv layers and a ReLU non-linearity layer. The total number of conv layers is 46. The decoder unit, which produces the reconstructed image, comprises the remaining nine modules, whereas the first nine modules compose the encoder unit, which provides the image segmentations. Extracts spatial features from each MRI slice illustrated in Eq. (9) [30]:

$$F_a = conv2D(I_t, W_s) + b_s (9)$$

Here, F_a denotes the spatial feature map, I_t is the MRI at time t, W_s is the spatial convolution weights and b_s is the bias term. Processes temporal dependencies between consecutive slices are illustrated in Eq. (10) [30]:

$$F_t = Conv1D(F_s, W_t) + b_t (10)$$

Where, F_t represents temporal feature representation, F_s are spatial features, W_t is the temporal convolution weights and b_t is a bias term. The W-Net structure applies U-Net-style downsampling and upsampling, as illustrated in Eq. (11), Eq. (12) [30]:

$$Z_e = Downsample(\sigma(Conv2D(F_t)))$$
 (11)

where, Z_e denotes encoded feature representation, F_t represents the temporal feature map, σ define the activation function.

$$Z_d = Upsample(\sigma(Conv2D(Z_e)))$$
 (12)

where, Z_d defines the decoded feature map, Z_e is encoded features, $Conv2D(Z_e)$ is refines the compressed feature map with another convolution operation. The W-Net uses two main loss functions like reconstruction and soft-n-cut-loss in Eq. (13), Eq. (14), Eq. (15) [30].

$$M_{soft-Ncut}(W,N) = \sum_{n=1}^{N} \frac{cut (E_{n},W-E_{n})}{asso(E_{n},W)}$$
 (13)

$$= N - \sum_{n=1}^{N} \frac{assoc(E_n, E_n)}{assoc(E_n, W)}$$
(14)

$$M_{reconstr} = ||Y - V_{Dec}(V_{Enc}(Y, U_{Enc}), U_{Enc})||_{2}^{2}$$
 (15)

Here, $M_{soft-Ncut}(W,N)$ represents the soft normalized cut loss for a graph with weight matrix W and N, E_n defines the n^{th} segment of the data. $cut\ (E_n,W-E_n)$ represents the sum of edge weights between segment E_n and the rest of the graph and $asso(E_n,W)$ defines total association E_n with W. $assoc(E_n,E_n)$ shows the total intra-cluster similarity. $M_{reconstr}$ defines reconstruction loss, Y represents the original input, V_{Enc} represents the encoder function, and U_{Enc} represents the decoder function.

In WNet, different types of graph nodes may require distinct feature vectors, which cannot always be represented by a fixed length. To address this, nodes are grouped into clusters based on feature length, and Spatial Graph Convolutional Networks (GCN) are

applied to convert these variable-length features to a uniform representation. This allows for consistent learning and segmentation of WM structures across MRI sequences.

IV. Result

This section evaluates performance in terms of several evaluation criteria and analyzes the assessment outcomes of the osteoporosis detection. osteoporosis detection and classification is found using the Python programming language and libraries (Sci-Kit-Learn, TensorFlow, Keras, Numpy, HDF5, etc.) on an Intel Core i7 processor running Windows with 16 GB of RAM.

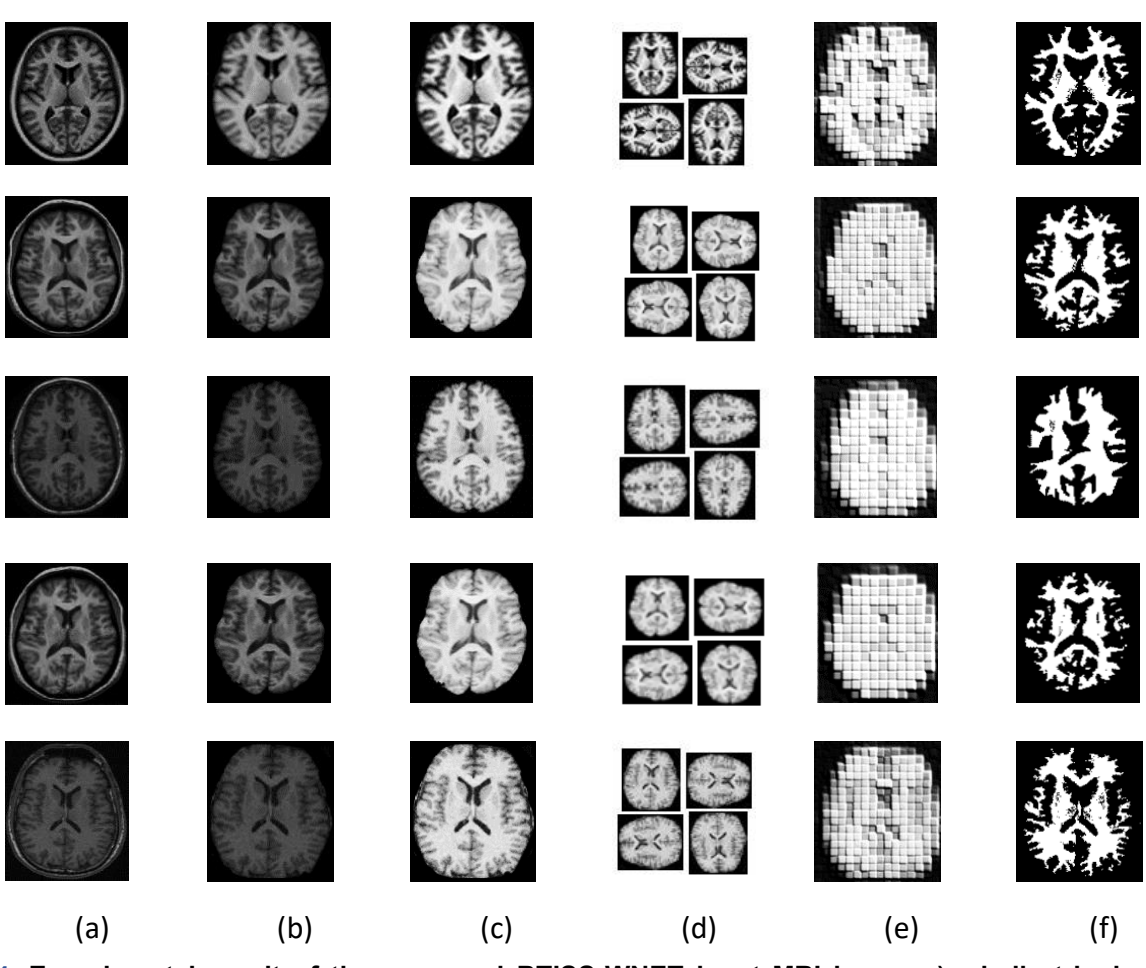


Fig. 4. Experimental result of the proposed BTISS-WNET input MRI image a), skull stripping b), preprocessing c), data augmentation d), feature extraction e) and segmentation f)

A. Performance Analysis

Evaluation measures were employed to verify the efficacy and characteristics of the proposed approach. True Negative $(True^{-})$, False Positive $(False^{+})$, True Positive (True⁺) and False Negative (False⁻) are the four basic metrics used to assess performance. They are illustrated as Eq. (16), Eq. (18), Eq. (19), Eq. (21), Eq. (22) [31], and Eq (17) and Eq. (20) [32].

$$Specificity = \frac{T_{neg}}{T_{neg} + F_{pos}} \tag{16}$$

$$Precision = \frac{T_{pos}}{T_{pos} + F_{pos}} \tag{17}$$

$$Recall = \frac{T_{pos}}{T_{pos} + F_{neg}} \tag{18}$$

$$Accuracy = \frac{T_{pos} + T_{neg}}{Total \ no.of \ samples}$$
(19)

$$F1 \ score = 2(\frac{Precision + Recall}{Precision + Recall})$$
(20)

$$Dice \ score = \frac{2T_{pos}}{F_{pos} + 2T_{pos} + F_{neg}}$$
(21)

$$F1 \ score = 2\left(\frac{Precision + Recall}{Precision + Recall}\right) \tag{20}$$

$$Dice\ score\ = \frac{2T_{pos}}{F_{pos} + 2T_{pos} + F_{reg}} \tag{21}$$

$$Jaccard\ index = \frac{T_{pos}}{T_{pos} + F_{neg} + F_{pos}}$$
 (22)

where T_{neg} and T_{pos} specifies true negatives and true positives of the sample images, F_{neg} and F_{pos} specifies false negatives and false positives of the sample images.

Fig. 5(a) displays the accuracy graph used in the proposed system's training and testing. Compared to

the training phase, the proposed method obtains greater accuracy during testing. As a result, the proposed framework operates more effectively. Fig. 5 (b) displays the loss graph for training and testing. Testing experiences a lower loss rate than training, which naturally raises accuracy.

B. Comparative Analysis

In this section, the experimental results of the suggested BTISS-WNET focusing on a comparison of its performance with other segmentation methods.

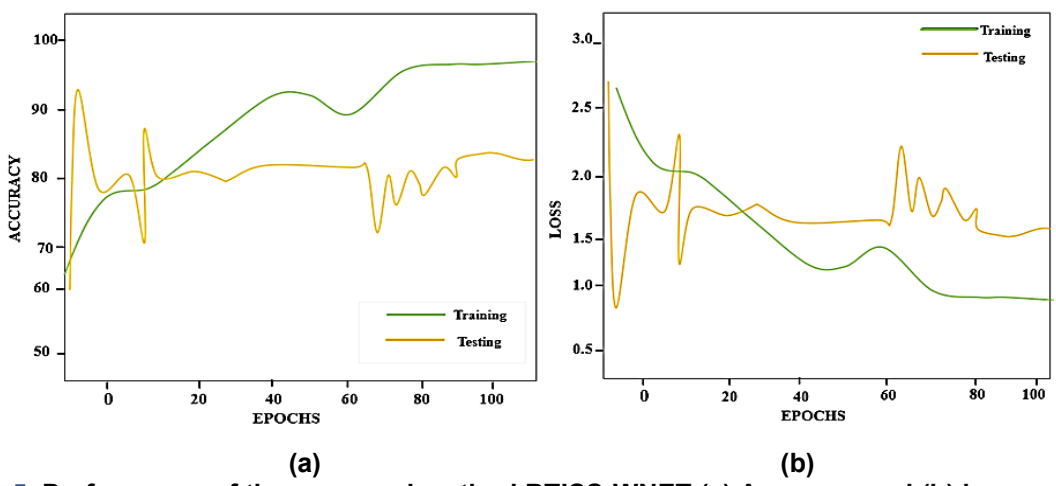


Fig. 5. Performance of the proposed method BTISS-WNET (a) Accuracy and (b) loss graph

Table.1. Comparison of Segmentation approaches

Methods	DI	JI
Graphcut [33]	91.67	92.80
SegNet [34]	93.32	91.25
U-Net [35]	95.05	94.36
V-Net [36]	97.81	96.41
Spatio temporal WNet	98.54	97.82

Table 1 illustrates the comparison of various segmentation algorithms with the Spatio-temporal WNet based on DI and JI metrics. The proposed Spatio-temporal WNet increases the overall DI by 7.49%, 5.59%, 3.67%, and 0.74% for Graphcut [33], SegNet [34], U-Net [35], and V-Net [36], respectively. According to the Table.1, Spatio-temporal WNet has the highest DI (98.54) and JI (97.82) scores among Graphcut, SegNet, U-Net, and V-Net algorithms, From this analysis, the proposed Spatio-temporal WNet indicates the best segmentation performance. Fig. 6 compares different methods for BTISS in MRI images. The image presents a comparative analysis of brain MRI segmentation methods: Graphcut [33], U-Net [35], V-Net [36], and the proposed Spatio-temporal WNet. Each row corresponds to a different MRI image, while each column represents segmentation results from a different method. A qualitative assessment of the segmentation result highlights the efficacy of the proposed BTISS-WNET in comparison with Graphcut, U-Net, and V-Net. The BTISS-WNET consistently delivers clearer and more anatomically accurate WM boundaries, while Graphcut results appear fragmented and incomplete. U-Net often blurs tissue edges, and V-Net introduces minor artifacts despite better localization. In contrast, BTISS-WNET effectively preserves fine structural details and handles intensity inhomogeneity with greater robustness. The visual clarity and consistency of BTISS-WNET outputs highlight its superior generalization and clinical reliability for BTISS. The performance of existing methods was assessed with the proposed framework to establish that the suggested strategy produces more effective outcomes. The F1, SP, and AC are used to evaluate performance. The accuracy rate obtained by the proposed framework is more efficient than the existing models. A comparative analysis has been performed between the proposed framework and the four existing methods, such as RegNet [35], ResNet [36], MobileNet [37], and GoogleNet [38].

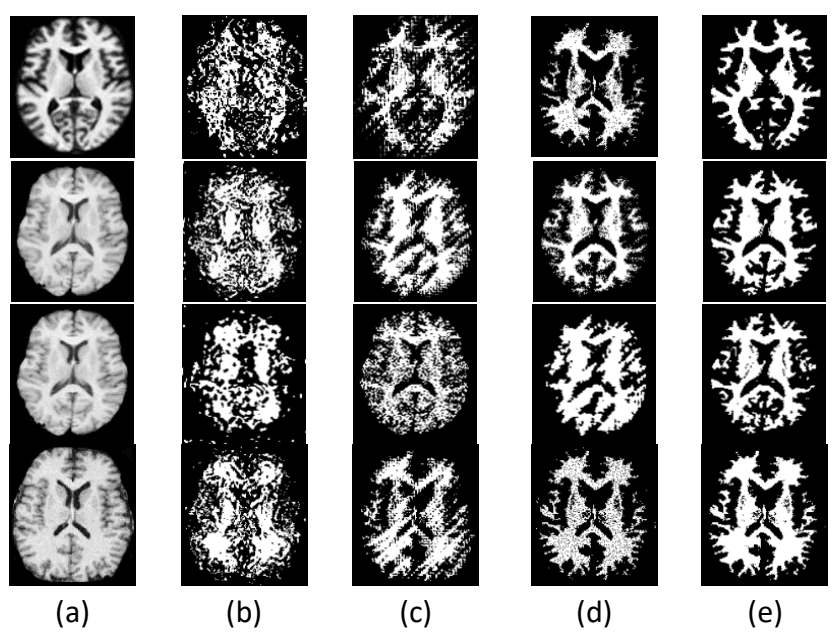


Fig. 6. Visualization results of different segmentation techniques input image (a), Graphcut (b), U-Net (c), V-Net (d) and spatio temporal WNet (ours) (e)

Table. 2. Comparison of existing techniques and proposed technique

Techniques	AC	SP	PR	RE	F1	P -value
RegNet [37]	93.65	91.04	95.23	92.2	90.55	0.056
ResNet [38]	97.18	94.78	91.4	95.53	91.32	0.072
MobileNet [39]	94.41	96.2	91.45	95.28	94.22	0.063
GoogleNet [40]	98.04	92.86	95.57	90.51	93.72	0.070
Proposed RGNet	99.32	97.49	92.87	93.3	96.1	0.051

Table 2 performance compared to the proposed BTISS-WNET approach and existing techniques such as RegNet [37], ResNet [38], MobileNet [39], and GoogleNet [40]. The proposed RGNet maintains a 99.32% high accuracy range. RGNet achieves an accuracy rate that is more efficient than that of existing The proposed RGNet improves its approaches. accuracy by 6.05%, 2.20%, 5.20% and 1.30% better than RegNet [37], ResNet [38], MobileNet [39], and GoogleNet [40], respectively. The reported p-values from paired t-tests are all below 0.051, indicating that the performance improvements of BTISS-WNET are statistically significant. Fig. 7 shows the assessment of the existing network with the suggested network. Table 3 presents a performance comparison of various DL architectures, RegNet, ResNet, MobileNet, GoogleNet, and the proposed RGNet, using MSE and RMSE as evaluation metrics. Among the models, the proposed RGNet achieves the lowest Mean Squared Error (MSE) (0.14) and Root Mean Squared Error (RMSE) (0.23), demonstrating superior AC and minimal prediction error. These results clearly establish the effectiveness of the proposed RGNet in enhancing prediction AC over conventional architectures. Table 4 demonstrates the impact of data augmentation on the performance of a DL model, comparing two key metrics: AC and F1. With augmentation, the model attained an AC of 99.32% and an F1 of 96.10% reflecting improved prediction reliability and balanced RE and PR. In contrast, without augmentation, the accuracy dropped to 98.12% and the F1 score fell to 90.23% indicating weaker generalization and class prediction. This highlights that augmentation significantly enhances the model's performance and robustness. An ablation study was conducted to evaluate each module in the BTISS-WNET framework by selectively removing key modules: EWT for pre-processing, the RGNet for feature extraction, and the Spatio-temporal WNet for seamentation. impact seamentation The on performance was measured using PR, RE, and AC metrics. Table 5 presents a comparative analysis of the proposed BTISS-WNET model under different ablation scenarios to assess the contribution of each

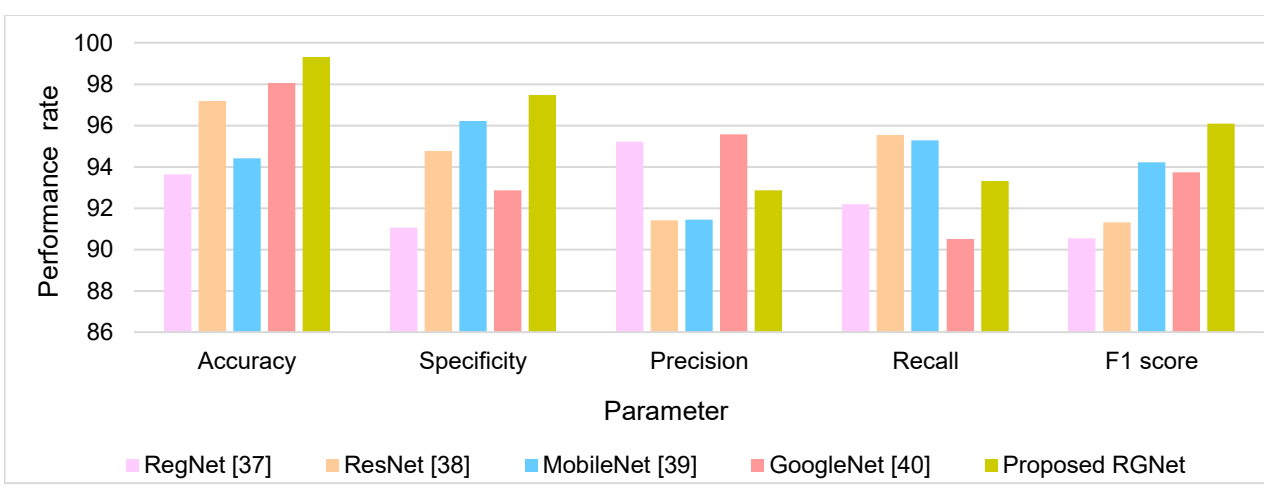


Fig. 7. Comparison of existing DL network with RGNet

component, like EWT, RGNet, and Spatio-temporal WNet, toward overall performance. The metrics used for evaluation include PR, RE, and AC. The full model configuration with all three components (EWT + RGNet + WNet) achieves the highest scores across all metrics, confirming the synergistic benefit of integrating preprocessing, feature extraction, and segmentation modules.

V. Discussion

The proposed BTISS-WNET model significantly advances BTISS, particularly in WM regions. The integration of EWT for pre-processing enhanced contrast and minimized noise, which improved tissue differentiation. The novel RGNet architecture, combining the strengths of ResNet [26] and GoogleNet [27], achieved a 6.05%, 2.20%, 5.20%, and 1.30% accuracy improvement over RegNet, ResNet, MobileNet, and GoogleNet, respectively. Furthermore,

98.54% and JI of 97.82% scores in WM segmentation further validate the model's robustness. In Table 2, the reported p-values from paired t-tests are below 0.051, indicating that the performance improvements of BTISS-WNET are statistically significant. The spatiolearning allowed precise boundary identification while reducing false positives, illustrating BTISS-WNET for clinical interpretation. Table 6 relates the AC of the proposed BTISS-WNET with existing methods such as DDSeg [41], BISON [42], and HMRF-WOA [43], respectively. The proposed BTISS-WNET model achieves an overall accuracy of 1.76%, 18.23% and 16.02% compared to the existing methods, such as DDSeg, BISON, and HMRF-WOA. The BTISS-WNET achieves a balanced trade-off with 6.2 million parameters and an average inference time of 12.7 ms. This study validates that the proposed method maintains practical computational effectiveness and is suitable for real-time applications. This improvement highlights the superior performance of BTISS-WNET in

Table. 3. Comparison of error rate with existing techniques and proposed technique

Methods	MSE	RMSE
RegNet [37]	0.45	0.56
ResNet [38]	0.53	0.87
MobileNet [39]	0.36	0.34
GoogleNet [40]	0.20	0.41
Proposed RGNet	0.14	0.23

the spatial-temporal WNet enabled the model to capture dynamic structural variations in MRI slices, resulting in a segmentation accuracy of 99.32%. This outperformed previous architectures such as DDSeg [41], BISON [42], and HMRF-WOA [43] by 1.76%, 18.23%, and 16.02%, respectively. Superior DI of

terms of classification AC. The results indicate that BTISS-WNET is more reliable and effective than the other models, making it a better choice for segmenting the WM cases with a high accuracy rate. Despite its strong performance, the proposed BTISS-WNET model has certain limitations.

Table. 4. Performance comparison of the BTISS-WNET model with and without augmentation

Metrics	With augmentation	Without augmentation
AC	99.32%	98.12%
F1	96.10%	90.23%

Table 5. Ablation Study of BTISS-WNET Components on Segmentation Performance

Metrics	Without EWT with	Without RGNet with	Without WNet with	With EWT+RGNet
	RGNet and WNet	EWT and WNet	RGNet and EWT	+WNet
PR	90.12%	91.53%	89.04%	92.87%
RE	87.05%	90.18%	91.75%	93.30%
AC	90.43%	97.75%	95.28%	99.32%

Table. 6. Comparison of existing methods versus proposed BTISS-WNET

Authors	Approaches	AC	Parameters (Millions)	Inference Time (ms)
Zhang, F., et al., [41] (2021)	DDSeg	97.6%	10.5	15.3
Dadar, M. et al., [42] (2021)	BISON	84%	8.4	18.5
Daoudi, A. et al., [43] (2024)	HMRFWOA	85.6%	7.8	13.9
Proposed	BTISSWNET	99.32%	6.2	12.7

First, its dependency on high-quality pre-processing may restrict robustness when applied to low-quality or artifact-prone MRI scans frequently encountered in clinical practice. Second, the spatio-temporal WNet introduces computational complexity, which may real-time deployment low-resource hinder in environments. These constraints suggest that while the model demonstrates high accuracy under controlled conditions, its translation to routine clinical workflows requires further optimization and external validation. Furthermore, the model has been tested only on the BrainWeb dataset, which may limit generalizability to diverse clinical datasets. Future work should therefore focus on validating the framework across multi-center, multi-modal MRI data to enhance its applicability in broader healthcare settings. In addition, explainable Al techniques could be incorporated to improve transparency and build clinical trust in automated segmentation outcomes. Finally, exploring lightweight architectures or model compression strategies may help reduce computational demands and facilitate wider adoption. The implications of this study are significant for both research and clinical practice. The BTISS-WNET framework, proposed integrating empirical wavelet-based preprocessing, hybrid Res-GoogleNet feature extraction, and spatio-temporal segmentation, demonstrates that deep learning models can achieve highly accurate and robust white matter segmentation in MRI scans. Accurate tissue segmentation not only enhances diagnostic reliability

but also supports downstream tasks such as disease monitoring, treatment planning, and prognosis evaluation in neurological disorders [44]. Recent surveys have emphasized that deep learning-based segmentation methods can reduce manual effort, improve reproducibility, and accelerate neuroimaging workflows in both research and clinical environments [45], [46]. Moreover, this model's relatively low parameter count and fast inference time suggest potential applicability in real-time or resource-limited healthcare settings, aligning with the growing demand for Al-assisted radiology [47]. By providing consistent and high-precision segmentation, BTISS-WNET could be integrated into large-scale brain MRI studies, clinical decision support systems, and longitudinal monitoring of patients with multiple sclerosis. Alzheimer's disease. and traumatic brain injury [48], [49].

VI. Conclusion

This research proposed a novel BTISS-WNET for BTISS using MRI images. The brain MRI images are fed into skull stripping to remove skull regions, and EWT is used for pre-processing to expand the image quality and noise reduction. The augmented MRI images are fed into RGNet to extract the features. The proposed method uses Spatio-temporal WNet for segmenting the WM in MRI images. The proposed RGNet improves its accuracy by 6.05%, 2.20%, 5.20% and 1.30% better than RegNet, ResNet, MobileNet, and GoogleNet. As a result of the experiment, the

Journal of Electronics, Electromedical Engineering, and Medical Informatics

Homepage: jeeemi.org; Vol. 8, No. 1, January 2026, pp: 1-15 e-ISSN: 2656-8632

the proposed method performed 99.32% more accurately than existing methods for segmenting the WM. The proposed BTISS-WNET model achieves an overall accuracy of 1.76%, 18.23% and 16.02% compared to the existing methods such as DDSeg, BISON, and HMRF-WOA. Future work will focus on validating the model using real clinical datasets and extending it for multi-tissue and multi-modal MRI segmentation.

Acknowledgment

The author would like to express his heartfelt gratitude to the supervisor for his guidance and unwavering support during this research for his guidance and support.

Funding

Not applicable.

Data Availability

Data sharing not applicable to this article as no datasets were generated or analyzed during the current study.

Author Contribution

Athur Shaik Ali Gousia Banu conceptualized and designed the study, collected data, and participated in data analysis and interpretation. Sumit Hazra contributed to the educational media's development, oversaw the intervention's implementation, and contributed to manuscript writing and revisions. Athur Shaik Ali Gousia Banu and Sumit Hazra assisted with data analysis and interpretation and provided critical feedback on the manuscript. All authors reviewed and approved the final version of the manuscript, as well as agreed to be responsible for all aspects of the work, ensuring integrity and accuracy.

Declarations

Ethical Approval

The research guide reviewed and ethically approved this manuscript for publication in the Journal.

Consent for Publication Participants.

Not applicable.

Competing Interests

The authors declare has no conflict of interest related to this publication.

References

[1] L. Wu, S. Wang, J. Liu, L. Hou, N. Li, F. Su, X. Yang, W. Lu, J. Qiu, M. Zhang, & L. Song, "A survey of MRI-based brain tissue segmentation using deep learning," Complex & Intelligent

- *Systems*, vol. 11, no. 1, pp. 1-16, 2025. doi: 10.1007/s40747-024-01639-1
- Q.U. Mastoi, S. Latif, S. Brohi, J. Ahmad, A. [2] Alghatani, M.S. Alshehri, A. Al Mazroa, & R. Ullah, "Explainable AI in medical imaging: an interpretable and collaborative federated learning model for brain tumor classification," Frontiers in Oncology, vol. 15, pp. 1535478-1535478. 2025. 10.3389/fonc.2025.1535478
- [3] K. Sailunaz, S. Alhajj, T. Özyer, J. Rokne, and R. Alhajj, "A survey on brain tumor image analysis," *Medical & Biological Engineering & Computing*, vol. 62, no. 1, pp. 1-45, 2024. doi: 10.1007/s11517-023-02873-4
- [4] Z. Liu, L. Tong, L. Chen, Z. Jiang, F. Zhou, Q. Zhang, X. Zhang, Y. Jin, and H. Zhou, "Deep learning-based brain tumor segmentation: a survey," *Complex & intelligent systems*, vol. 9, no. 1, pp. 1001-1026, 2023. doi: 10.1007/s40747-022-00815-5
- [5] R. Palaniappan, and S. Rathinavelayutham, "Digital Twin-Assisted Deep Learning with Model Fusion for Detecting Multiple Sclerosis in MRI Modalities," Journal of Data Science and Intelligent Systems, 2025. doi: 10.47852/bonviewjdsis52024391
- [6] C. John Clementsingh and S. Sumathi, "Face Regeneration and Recognition using Deep Learning based Sift-Hog Assisted Gan Model", International Journal of Data Science and Artificial Intelligence, vol. 02, no.05, pp. 142-148, 2024.
- [7] Cheepurupalli Raghuram, V. S. R. K. Raju Dandu, and DR. B. Jaison, "Hybridization of Dilated Cnn with Attention Link Net for Brain Cancer Classification," *International Journal of Data Science and Artificial Intelligence*, vol. 02, no. 02, pp. 35-42, 2024.
- [8] R. Sundarasekar, and A. Appathurai, "FMTM-feature-map-based transform model for brain image segmentation in tumor detection," *Network Computing Neural Systems*, vol. 34, no. 1-2, pp. 1-25, 2023. doi: 10.1080/0954898x.2022.2110620
- [9] X. Huang, Y. Liu, Y. Li, K. Qi, A. Gao, B. Zheng, D. Liang, and X. Long, "Deep learning-based multiclass brain tissue segmentation in fetal MRIs," *Sensors*, vol. 23, no. 2, pp.655, 2023. doi: 10.3390/s23020655
- [10] R. Palaniappan, and S. Rathinavelayutham, "Digital Twin-Assisted Deep Learning with Model Fusion for Detecting Multiple Sclerosis in MRI Modalities," *Journal of Data Science and*

Manuscript received Marc 8, 2025; Revised August 20, 2025; Accepted September 1, 2025; date of publication December 4, 2025 Digital Object Identifier (**DOI**): https://doi.org/10.35882/jeeemi.v8i1.808

Copyright © 2025 by the authors. This work is an open-access article and licensed under a Creative Commons Attribution-ShareAlike 4.0 International License (CC BY-SA 4.0).

- Intelligent Systems, 2025. doi: 10.47852/bonviewjdsis52024391
- [11] R. Abirami, and P. Krishna Kumar, "Deep Learning Model for Accurate Brain Tumor Detection Using CT and MRI Imaging," International Journal of System Design and Computing, vol. 02, no. 01, pp. 26-31, 2024.
- [12] B. Thyreau, Y. Tatewaki, L. Chen, Y. Takano, N. Hirabayashi, Y. Furuta, J. Hata, S. Nakaji, T. Maeda, M. Noguchi-Shinohara, and M. Mimura, "Higher-resolution quantification of white matter hypointensities by large-scale transfer learning from 2D images on the JPSC-AD cohort," *Human Brain Mapping*, vol. 43, no. 13, pp. 3998-4012, 2022. doi: 10.1002/hbm.25899
- [13] A. Appathurai, A. S. I. Tinu, and M. Narayanaperumal, "Meg and Pet Images-Based Brain Tumor Detection Using Kapur's Otsu Segmentation and Sooty Optimized Mobilenet Classification," Revue Roumaine des Sciences Techniques Série Électrotechnique Et Énergétique, vol. 69, no. 3, pp. 359-364, 2024. doi: 10.59277/rrst-ee.2024.69.3.18
- [14] T. Magadza, and S. Viriri, "Deep learning for brain tumor segmentation: a survey of state-of-the-art," *Journal of Imaging*, vol. 7, no. 2, pp. 19, 2021. doi: 10.3390/jimaging7020019
- [15] R. Jin, D. Li, D. Xiang, L. Zhang, H. Zhou, F. Shi, W. Zhu, J. Cai, T. Peng, and X. Chen, "Al-based Automatic Segmentation of Prostate on Multimodality Images: A Review," arXiv preprint arXiv:2407.06612, 2024. doi: 10.21037/qims-24-723
- [16] N. Yamanakkanavar, and B. Lee, "Using a patch-wise m-net convolutional neural network for tissue segmentation in brain mri images," *IEEE Access*, vol. 8, pp. 120946-120958, 2020. doi: 10.1109/access.2020.3006317
- [17] M. Veluchamy, and B. Subramani, "Brain tissue segmentation for medical decision support systems," *Journal of Ambient Intelligence and Humanized Computing*, vol. 12, no. 2, pp. 1851-1868, 2021. doi: 10.1007/s12652-020-02257-8
- A. Cleriques, S. Valverde, J. Salvi, A. Oliver, and [18] X. Lladó, "Minimizing the effect of white matter lesions on deep learning-based segmentation for brain volumetry," Computerized Medical Imaging and Graphics, pp. 103, 102157. 2023. 10.1016/j.compmedimag.2022.102157
- [19] G. Park, J. Hong, B.A. Duffy, J.M. Lee, and H. Kim, "White matter hyperintensities segmentation using the ensemble U-Net with multi-scale highlighting foregrounds,"

- *Neuroimage*, vol. 237, pp. 118140, 2021. doi: 10.1016/j.neuroimage.2021.118140
- [20] N. Yamanakkanavar, and B. Lee, "A novel M-SegNet with global attention CNN architecture for automatic segmentation of brain MRI," Computers in Biology and Medicine, vol. 136, pp. 104761, 2021. doi: 10.1016/j.compbiomed.2021.104761
- [21] Z. Rieu, J. Kim, R.E. Kim, M. Lee, M.K. Lee, S.W. Oh, S.M. Wang, N.Y. Kim, D.W. Kang, H.K. Lim, and D. Kim, "Semi-supervised learning in medical MRI segmentation: brain tissue with white matter hyperintensity segmentation using FLAIR MRI," *Brain Sciences*, vol. 11, no. 6, pp. 720, 2021. doi: 10.3390/brainsci11060720
- [22] S. Kollem, "An efficient method for MRI brain tumor tissue segmentation and classification using an optimized support vector machine," Multimedia Tools Applications, vol. 83, no. 26, pp. 68487-68519, 2024. doi: 10.1007/s11042-024-18233-9
- [23] S. Gudise, K. Giri Babu, & T. Satya Savithri, "An advanced fuzzy C-Means algorithm for the tissue segmentation from brain magnetic resonance images in the presence of noise and intensity inhomogeneity," *The Imaging Science Journal*, vol. 72, no. 4, pp. 520-539, 2024. doi: 10.1080/13682199.2023.2210400
- [24] S. Mohapatra, G.K. Pati, M. Mishra, and T. Swarnkar, "Gastrointestinal abnormality detection and classification using empirical wavelet transform and deep convolutional neural network from endoscopic images," Ain Shams Engineering Journal, vol. 14, no. 4, pp. 101942, 2023. doi: 10.1007/s12539-021-00417-8
- [25] V. Chamola, and P. Narang, "AGD-Net: Attention-Guided Dense Inception U-Net for Single-Image Dehazing," 2023. doi: 10.1007/s12559-023-10244-2
- V. Rathinam, R. Arunagiri, V. Krishnasamy, and [26] Rajendran, "Tri-level lung cancer classification deep learning based via with computed GoogleNet tomography images," Bulletin of Electrical Engineering and Informatics, vol. 14, no. 3, pp. 2198-2208, 2025. doi: 10.11591/eei.v14i3.9258
- [27] M. Talele, and R. Jain, "A Comparative Analysis of CNNs and ResNet50 for Facial Emotion Recognition," Engineering, Technology & Applied Science Research, vol. 15, no. 2, pp. 20693-20701, 2025. doi: 10.48084/etasr.9849
- [28] W. Xu, Y.L. Fu, and D. Zhu, "ResNet and its application to medical image processing: Research progress and challenges," Computer Methods and Programs in Biomedicine, vol. 240,

Journal of Electronics, Electromedical Engineering, and Medical Informatics

Homepage: jeeemi.org; Vol. 8, No. 1, January 2026, pp: 1-15 e-ISSN: 2656-8632

- pp. 107660, 2023. doi 10.1016/j.cmpb.2023.107660
- [29] M. Grammatikopoulou, R. Sanchez-Matilla, F. Bragman, D. Owen, L. Culshaw, K. Kerr, D. Stoyanov, and I. Luengo, "A spatio-temporal network for video semantic segmentation in surgical videos," *International Journal of Computer Assisted Radiology and Surgery*, vol. 19, no. 2, pp. 375-382, 2024. doi: 10.1007/s11548-023-02971-6
- [30] B.M. Anderson, B. Rigaud, Y.M. Lin, A.K.Jones, H.C. Kang, B.C. Odisio, and K.K. Brock, "Automated segmentation of colorectal livermetastasis and liver ablation on contrastenhanced CT images," Frontiers inOncology, vol. 12, pp. 886517, 2022. doi: 10.3389/fonc.2022.886517
- [31] Alqhtani, S.M., Soomro, T.A., Shah, A.A., Memon, A.A., Irfan, M., Rahman, S., Jalalah, M., Almawgani, A.H. and Eljak, L.A.B., 2024. Improved brain tumor segmentation and classification in brain MRI with FCM-SVM: a diagnostic approach. IEEE Access, vol. 12, pp.61312-61335.
- [32] Almufareh, M.F., Imran, M., Khan, A., Humayun, M. and Asim, M., 2024. Automated brain tumor segmentation and classification in MRI using YOLO-based deep learning. IEEE Access, vol. 12, pp.16189-16207.
- [33] Y. Ghasemipour, and M. Niazi, 2025. Image segmentation enhancement using aggregated kernel graph cut. *Signal Processing and Renewable Energy (SPRE)*, vol. 9, no. 1, 2025. doi: 10.1007/s11760-023-02546-7
- [34] V.S.D. Tejaswi, and V. Rachapudi, "Computer-aided diagnosis of liver cancer with improved SegNet and deep stacking ensemble model," *Computational Biology and Chemistry*, vol. 113, pp. 108243, 2024. doi: 10.1016/j.compbiolchem.2024.108243
- [35] Z. Wang, S. Fu, H. Zhang, C. Wang, C. Xia, P. Hou, C. Shun, and G. Shun, "Dual-branch dynamic hierarchical U-Net with multi-layer space fusion attention for medical image segmentation," *Scientific Reports*, vol. 15, no. 1, pp. 8194, 2025. doi: 10.1038/s41598-025-92715-0
- [36] F. Turk, and M. Kılıçaslan, "Lung image segmentation with improved U-Net, V-Net and Seg-Net techniques," *PeerJ Computer Science*, vol. 11, pp. e2700, 2025. doi: 10.7717/peerj-cs.2700
- [37] T. Chauhan, V. Katkar, and K. Vaghela, "Corn leaf disease detection using RegNet, KernelPCA and XGBoost classifier," In *International*

- Conference on Advancements in Smart Computing and Information Security, pp. 346-361, 2022. doi: 10.1007/978-3-031-23092-9 28
- [38] T.S. Priya, and T. Ramaprabha, "Resnet based feature extraction with decision tree classifier for classification of mammogram images," *Turkish Journal of Computer and Mathematics Education*, vol. 12, no. 2, pp. 1147-1153, 2021. doi: 10.17762/turcomat.v12i2.1136
- [39] A.W. Al-funjan, H.M. Al Abboodi, N.A. Hamza, W.M.S. Abedi, and A.H. Abdullah, "A Lightweight Deep Learning-Based Ocular Disease Prediction Model Using Squeeze-and-Excitation Network Architecture with MobileNet Feature Extraction," International Journal of Intelligent Engineering & Systems, vol. 17, no. 4, 2024. doi: 10.22266/ijies2024.0831.19
- [40] A.W. Al-funjan, H.M. Al Abboodi, N.A. Hamza, W.M.S. Abedi, and A.H. Abdullah, "A Lightweight Deep Learning-Based Ocular Disease Prediction Model Using Squeeze-and-Excitation Network Architecture with MobileNet Feature Extraction," *International Journal of Intelligent Engineering & Systems*, vol. 17, no. 4, 2024. doi: 10.22266/ijies2024.0831.19
- [41] F. Zhang, A. Breger, K.I.K. Cho, L. Ning, C.F. Westin, L.J. O'Donnell, and O. Pasternak, "Deep learning-based segmentation of brain tissue from diffusion MRI," *NeuroImage*, vol. 233, pp. 117934, 2021. doi: 10.1016/j.neuroimage.2021.117934
- [42] M. Dadar, and D.L. Collins, "BISON: Brain tissue segmentation pipeline using T1-weighted magnetic resonance images and a random forest classifier," *Magnetic Resonance in Medicine*, vol. 85, no. 4, pp. 1881-1894, 2021. doi: 10.1002/mrm.28547
- [43] A. Daoudi, and S. Mahmoudi, "Enhancing Brain Segmentation in MRI through Integration of Hidden Markov Random Field Model and Whale Optimization Algorithm," *Computers*, vol. 13, no. 5, pp. 124, 2024. doi: 10.3390/computers13050124.
- [44] L. Wu, S. Wang, J. Liu, L. Hou, N. Li, F. Su, X. Yang, W. Lu, J. Qiu, M. Zhang, L. Song, "A survey of MRI-based brain tissue segmentation using deep learning," *Complex & Intelligent Systems*, vol. 11, no. 1, pp. 1–16, 2025. doi: 10.1007/s40747-024-01639-1
- [45] Z. Liu, L. Tong, L. Chen, Z. Jiang, F. Zhou, Q. Zhang, X. Zhang, Y. Jin, H. Zhou, "Deep learning-based brain tumor segmentation: a survey," *Complex & Intelligent Systems*, vol. 9, no. 1, pp. 1001–1026, 2023. doi: 10.1007/s40747-022-00815-5

- [46] T. Magadza, S. Viriri, "Deep learning for brain tumor segmentation: a survey of state-of-the-art," *Journal of Imaging*, vol. 7, no. 2, pp. 19, 2021. doi: 10.3390/jimaging7020019
- [47] R. Palaniappan, S. Rathinavelayutham, "Digital Twin-Assisted Deep Learning with Model Fusion for Detecting Multiple Sclerosis in MRI Modalities," Journal of Data Science and Intelligent Systems, 2025. doi: 10.47852/bonviewjdsis52024391
- [48] X. Huang, Y. Liu, Y. Li, K. Qi, A. Gao, B. Zheng, D. Liang, X. Long, "Deep learning-based multiclass brain tissue segmentation in fetal MRIs," *Sensors*, vol. 23, no. 2, pp. 655, 2023. doi: 10.3390/s23020655
- [49] B. Thyreau, Y. Tatewaki, L. Chen, Y. Takano, N. Hirabayashi, Y. Furuta, J. Hata, S. Nakaji, T. Maeda, M. Noguchi-Shinohara, M. Mimura, "Higher-resolution quantification of white matter hypointensities by large-scale transfer learning from 2D images on the JPSC-AD cohort," *Human Brain Mapping*, vol. 43, no. 13, pp. 3998–4012, 2022. doi: 10.1002/hbm.25899

Author Biography



Athur Shaik Ali Gousia Banu Assistant Professor at Muffakham Jah College of Engineering & Technology (MJCET), is a highly accomplished academician with over 30 years of teaching experience in Computer Science, Information

Technology, and Management. Holding a B. Tech (AMIE) in CSE, M. Tech (CSE), MBA (Systems), and a Ph.D. in MIS, she is currently pursuing her second Ph.D. in CSE. She is ratified by both Osmania University and JNTUH and has been recognized with the Ideal Teaching Award Programme (ITAP) in 2022. Her teaching spans from polytechnic institutions to undergraduate and postgraduate levels, covering B. Tech, M. Tech, MBA, MCA, and M. Phil. programs. Dr. Banu is known for her dynamic, student-friendly approach and passion for quality education, mentoring. and innovation. She has authored and edited several academic books and published over 44 research papers, including SCIE and Scopus-indexed works. With 13+ patents (2 granted), active involvement in NBA, NAAC, and AUTONOMOUS processes, and memberships in MIE and AIMERS, she is also an editorial board member and Associate Editor of Science Frontiers. A continuous learner, she has completed multiple FDPs, NPTEL courses, and online certifications, embodying academic excellence and professional dedication.



Sumit Hazra received his Ph.D. degree in Computer Science and Engineering from the National Institute of Technology (NIT) Rourkela, Odisha, in the year 2023. He received his M. Tech degree in Computer Science and Engineering

from VIT University, Vellore, India. He received his B.Tech degree in Computer Science and Engineering from WBUT (currently MAKAUT). He is currently working as an Assistant Professor & AI/ML Research Group Head in the Department of Computer Science and Engineering at Koneru Lakshmaiah Education Foundation, Hyderabad. He is also a prestigious member of IEEE and serves as a reviewer of several SCI/SCIE journals, e.g., IEEE Transactions on Cybernetics, Biomedical Signal Processing & Control, Cognitive Neurodynamics, Scientific Reports, etc. He is also a member of the IEEE Professional Body. He has organized several FDPs, Workshops, and has been an active member of various committees for several International Conferences. His research interests include Gait Analysis, Cognitive Science, Artificial Intelligence, Pattern Recognition, Computer Vision, and so on.